Improvement of OMI ozone profile retrievals by simultaneously fitting Polar Mesospheric Clouds

Juseon Bak[1] (sunnypark@pusan.ac.kr), Xiong Liu[2] (xliu@cfa.harvard.edu), Jae H. Kim[1] (jaekim@pusan.ac.kr), Matthew T. Deland[3] (matthew.deland@ssaihq.com), Kelly Chance[2] (kchance@cfa.harvard.edu)

1 Pusan National University, Department of Atmospheric Sciences, Busan, South Korea.
2 Harvard-Smithsonian Center for Astrophysics, Cambridge, MA, United States.
3 Systems and Applications, Inc. (SSAI), 10210 Greenbelt Rd., Suite 600, Lanham, MD 20706, USA

Abstract

The presence of polar mesospheric clouds (PMCs) in summer high latitudes could affect the retrieval of ozone profiles using backscattered ultraviolet (UV) measurements. PMC-induced errors in ozone profile retrievals from Ozone Monitoring Instrument (OMI) backscattered UV measurements are investigated through comparisons with Microwave Limb Sounder (MLS) ozone measurements. This comparison demonstrates that the presence of PMCs leads to systematic biases at pressures less than 6 hPa (~35 km); the biases increase from ~-2% at 2 hPa to ~-20% at 0.5 hPa on average, and are significantly correlated with brightness of PMCs. Sensitivity studies show that the radiance sensitivity to PMCs strongly depends on wavelength, increasing by a factor of ~4 from 300 nm to 265 nm. It also strongly depends on the PMC scattering, thus depending on viewing geometry. The optimal estimation-based retrieval sensitivity analysis shows that PMCs located at 80-85 km have the greatest effect on ozone retrievals at ~0.2 hPa (~60 km),

where the retrieval errors range from -2.5% with PMC optical depth (POD) of 10^{-4} to -20% with 10^{-3} at back scattering angles, and the impacts increase by a factor of ~5 at forward scattering angles due to stronger PMC sensitivities. To reduce the interference of PMCs on ozone retrievals, we perform simultaneous retrievals of POD and ozone with a loose constraint of 10^{-3} for POD, which results in retrieval errors of $1 - 4 \times 10^{-4}$. It is demonstrated that the negative bias of OMI ozone retrievals relative to MLS can be improved by including the PMC in the forward model calculation and retrieval.

1 Introduction

PMCs are tenuous layers of ice crystals that form at 80-85 km altitude only during the hemispheric summer season (~ 30 days before to ~ 65 days after summer solstice) at high latitudes and occasionally at mid-latitudes (Thomas et al., 1991; Taylor et al., 2002; DeLand et al., 2010). It has been suggested that the change of PMC properties such as frequency and brightness is linked to long-term changes in the composition and thermal structure of our atmosphere caused by human activities.

The mesospheric clouds in the daytime are detectable only from space, whereas ground-based observations are limited to immediately after sunset or before sunrise (DeLand et al., 2003). The optimal way to observe PMC from space is to employ limb-viewing sensors measuring the scattered solar radiation from which the cloud layers are easily identified as the enhanced radiances against the relatively weak atmospheric scattering (Thomas et al., 1991; Deland et al., 2006). The seasonal-latitudinal behaviors of PMC occurrence, brightness, altitude were characterized from various limb-viewing instruments including the Solar Mesosphere Explorer (SME), the Student nitric Oxide Explore (SNOE), and the SCanning Imagining Absorption spectroMeter for Atmospheric CHartographY (Olivero and Thomas, 1986; Bailey et al., 2005; von Savigny et al., 2004). These satellite measurements further contribute to understanding of microphysical properties of PMCs such as water vapor content, size distribution, and shape, which still remain a challenge (e.g., Thomas, 1984; Rapp et al., 2007; von Savigny and Burrows, 2007).

Even through nadir-viewing sensors could not provide information about the PMC altitude, Thomas et al. (1991) first demonstrated that PMCs are detectable from nadir-looking UV measurements using a brightness-based detection algorithm. PMC occurrence and residual albedo have been derived from Solar Backscatter Ultraviolet (SBUV, SBUV/2) and Ozone Monitoring Instrument (OMI) nadir UV measurements at shorter wavelengths below 300 nm where the Rayleigh-scattered background is comparatively low due to very strong ozone absorption. Thomas et al. (1991) found an anti-correlation of the PMC occurrence frequency with solar activity from 8 years of SBUV albedo data over the period 1978 to 1986. Further studies have demonstrated long-term trends over 30+ years in PMC occurrence frequency, brightness, particle radii, and ice water content (DeLand et al., 2003, 2007; Shettle et al., 2009; Hervig and Stevens, 2014; DeLand and Thomas, 2015). OMI PMC observations were used to characterize the local time variation of PMC occurrence frequency and brightness, with the advantage of overlapping pixels over the polar region due to the wide swath of OMI (Deland et al., 2011). On the other hand, the detectability of the signal of PMCs from UV wavelengths below 300 nm in the ozone Hartley bands implies that failure to account for PMCs in ozone profile retrievals using these wavelengths might affect the determination of ozone and its trends in the upper atmosphere from nadir-viewing UV instruments such as SBUV, SBUV/2, OMI, Global Ozone Monitoring Experiment (GOME) (ESA, 1995), SCIAMACHY, GOME-2 (Munro et al., 2006), and Ozone Mapping and Profiler Suite (OMPS) Nadir Profiler instruments (Flynn et al., 2014). However, the impact of PMCs on ozone retrievals has not been taken into account for any ozone algorithm or even thoroughly investigated with sufficient statistical data.

This paper is motivated by two main goals. The first objective is to identify the effect of PMCs on OMI ozone profile retrievals. For this purpose, we combine the OMI PMC detection algorithm of DeLand et al. (2010) and the OMI ozone profile retrieval algorithm of Liu et al. (2010a) and evaluate OMI ozone profiles for PMC and non-PMC pixels through comparison with collocated MLS measurements. The second one is to simultaneously retrieve the PMC optical depth with ozone using an optimal estimation technique, to reduce the interference on ozone profile retrievals.

In Sect. 2 we briefly introduce satellite measurements of OMI and MLS used in this study and then describe the PMC detection algorithm and the PMC optical depth (POD) retrieval algorithm, respectively. In Sect. 3.1 we evaluate OMI ozone profile retrievals (without POD retrievals) against MLS ozone profiles during the PMC season. Section 3.2 presents the results from a retrieval sensitivity study to see if OMI measurements provide adequate sensitivity to measure PMC optical depth. The improvement of ozone profile retrievals with simultaneously retrieved POD is discussed in Sect. 3.3. We summarize and conclude our results in Sect. 4.

2 Data and Methods

2.1 OMI and MLS Ozone measurements

Both the OMI and MLS instruments are on board the Aura satellite which is flown in a 705 km sun-synchronous polar orbit with ascending equator-crossing time at ~13:45 (Schoeberl et al., 2006). MLS measurements are taken about 7 minutes ahead of OMI for the same locations during daytime orbital tracks.

OMI is a nadir-viewing, ultraviolet-visible imaging spectrometer that measures backscattered radiances from 260 to 500 nm (UV-1: 260-310 nm; UV-2: 310-365 nm; VIS: 365-500 nm) at spectral resolutions of 0.42-0.63 nm with daily global coverage (Levelt et al., 2006). The spatial resolution is 13×24 km^2 for UV-2 and VIS and 13×48 km^2 for UV-1 at nadir position in the global mode. The OMI science teams provide two operational total ozone products, OMTO3 (Bhartia and Wellemeyer, 2002) and

OMDOAO3 (Veefkind et al., 2006), and one operational ozone profile product, OMO3PR (Kroon et al., 2011). We use the Smithsonian Astrophysical Observatory (SAO) ozone profile algorithm (Liu et al., 2010a) to deal with the error analysis of OMI ozone profile retrievals due to PMC contamination. This algorithm retrieves partial column ozone at 24 layers (surface to ~ 65 km) from OMI measurements with the fitting window of 270-330 nm, based on the well-known optimal estimation (OE) technique (Rodgers, 2000). The iterative solution of the nonlinear problem is given as:

$$\mathrm{X}_{\mathrm{i+1}} = X_i + (K_i^T S_y^{-1} K_i + S_a^{-1})^{-1}[K_i^T S_y^{-1}(Y - R(X_i)) - S_a^{-1}(X_i - X_a)] \qquad (1)$$

where $\mathrm{X}_{\mathrm{i+1}}$, X_i, X_a, and Y are the current and previous state vectors, a priori vector, and measured radiance vector (defined as logarithm of normalized radiance), respectively; $R(X_i)$ and K_i are the simulated logarithm of radiance spectrum and the weighting function matrix ($\partial \mathrm{R}/\partial \mathrm{X}_{\mathrm{i}}$) calculated using the Vector Linearized Discrete Ordinate Radiative Transfer model (VIDORT) (Spurr, 2006; 2008); the measurement error covariance matrix and a priori error covariance matrix are defined as S_{y} and S_{a}, respectively. Ozone a priori information is generally taken from climatological mean values and standard deviations of long-term measurements data, respectively. This iterative process is performed until the cost function χ^2 (Eq. 2) converges.

$$\chi^2 = \left\| S_y^{-\frac{1}{2}}\{K_i(\mathrm{X}_{\mathrm{i+1}} - X_i) - [Y - R(X_i)]\}\right\|_2^2 + \left\| S_a^{-\frac{1}{2}}(\mathrm{X}_{\mathrm{i+1}} - X_a)\right\|_2^2. \qquad (2)$$

where $\| \quad \|_2^2$ denote the the sum of each element squared.

The quality of the retrievals could be characterized by the solution error, defined as the root square sum of the random noise error and smoothing error. The vertical resolution estimated by Liu et al. (2010a) is ~ 7-11 km in stratosphere. The retrieval random-noise errors range from 1% in the middle stratosphere to 10% in the lower stratosphere, and the solution errors are typically 1-6% in the stratosphere

MLS is a forward-looking, thermal-emission, microwave limb sounder that takes measurements along-track and performs 240 limb scans per orbit with a footprint of ~ 6 km across-track and ~200 km along-track (Waters et al., 2006). The MLS ozone used here is the version 3.3 standard ozone product (55 pressure levels) retrieved from the 240 GHz radiance information, publicly available from the NASA Goddard Space Flight Center Earth Sciences (GES) data and Information Services Center (DISC). The typical vertical resolution of this product is 2.5-3.5 km from 261 to 0.2 hPa and 4-5.5 km from 0.1 to 0.02 hPa; the precision is estimated to be a few% in the middle stratosphere, but 5-100% below 150 hPa and 60-300% above 0.1 hPa. We apply all the data screening criteria recommended in Livesey et al. (2011) and hence limit MLS ozone data to "quality" higher than 0.6, "convergence" lower than 1.18, positive "*precision*" values and even "status" value for the pressure range of 261-0.02 hPa.

Liu et al. (2010b) used the v2.2 MLS ozone data to validate the OMI ozone profile retrievals and demonstrated the excellent OMI/MLS agreement of within 4% in the middle stratosphere, except for positive biases of 5-10% above 0.5 hPa and negative biases of 10-15% below 100 hPa, which are greatly improved by accounting for OMI's coarser vertical resolution using OMI averaging kernels.

2.2 OMI PMC detection

The flag data to detect both PMC and non-PMC regions from OMI measurements are provided by DeLand et al. (2010). This detection algorithm uses albedo data (A = I/F, I= radiance, F=irradiance) at 267, 275, 283.5, 287.5, and 292.5 nm after interpolating all spectra to a 0.5 nm grid and averaging three consecutive bins. The PMC pixels are identified using enhancements above the Rayleigh scattering background. The background atmospheric albedo due to Rayleigh scattering and ozone absorption (A_{ray}) is determined using a 4th order fit in solar zenith angle to non-PMC pixels for each orbit, after applying a geometric adjustment for cross-track albedo variations as defined in Eq. (4) of DeLand et al. (2010). Positive signals of albedo residuals ($A - A_{ray}$) could be induced by “false PMCs” including random instrument noise and geophysical variability of ozone as well as by the PMC scattering. The minimum residual albedo value for PMC detection is derived from measurements of clear atmospheric variability, and is adjusted to eliminate false PMC signal due to instrument noise. The false PMC signal due to a negative ozone deviation is screened out using the wavelength-dependence of PMC signals that become stronger at shorter wavelengths. The PMC are typically observed at latitudes above 55° from OMI where Solar Zenith Angle (SZA)s are above ~35°, Viewing Zenith Angle (VZA)s are below ~ 70°, relative AZimuth Angle (AZA)s range from ~ 40° to ~80° (right side of the nadir swath) and from ~ 110° and ~ 130° (left side of the nadir swath), depending on the cross-track position.

2.3 PMC optical depth retrievals

In the standard ozone retrieval mode, the atmosphere is divided into 24 layers; the bottom level of a layer i is defined as $P_i = 2^{-\frac{(i-1)}{2}} \times 1013.15\, hPa$ with the top of atmosphere, the upper level of layer 24, set at 0.087 hPa (~65 km). Radiance calculations are made using the VLIDORT model for a Rayleigh atmosphere (no aerosol) assuming Lambertian reflectance for ground surface and for clouds.

Due to the well-defined spatiotemporal range for PMCs, we will first detect PMCs using the PMC detection algorithm specified in Sect. 2.2, and then calculate weighting functions for POD and include them in the state vector with loose constraints. In the POD retrieval mode, we add five more layers between ~65 km and ~90 at 5km intervals; the bottom level of a layer i is defined as $P_i = 10^{-(\frac{(i-25)\times 5+65}{16})} \times 1013.15\, for\ i = 25, \ldots 29$. A PMC layer is inserted to the single layer of 80-85 km. Simulating the scattering particles in the radiative process requires the specification of a particle size distribution, the distribution size, and the distribution dispersion width, and a particle shape. The primary component of the PMC particles was first confirmed as non-spherical ice crystals by Hervig et al. (2001). The range of reported radii and size distribution widths is 15-100 nm and 10-20 nm and log-normal or Gaussian size distributions are normally assumed (Englert et al., 2007; Hervig et al., 2009). In this study, PMCs are assumed to be spherical ice particles with a log-normal size distribution ($\mathrm{r_o} = 55\,nm, \sigma_g = 1.4$), so that Mie theory can be used, because the particle shape plays a minor role in the UV scattering (Baumgarten and Thomas, 2005; Eremenko et al., 2005). The ice refractive index, $1.33 + 5 \times 10^{-9}i$ at 300 nm from Warren (1984), was used for the entire wavelength range because of low dependence on UV wavelength. The temperature profile is taken from daily National Centers for Environmental Prediction (NCEP) final (FNL) Operational Global analysis data (http://rda.ucar.edu/datasets/ds083.2/) below 10 hPa and from climatological data above. We take ozone a priori information from monthly and zonal mean ozone profile climatology presented in McPeters and Labow (2012), which is based on the Aura MLS v3.3 data (2004-2010) and ozonesonde data (1988-2010). Climatological a priori information for PMC optical thickness is not available. It is selected here by trial and error. As a result, the a priori state and its error are set to be 0 and 10^{-3}, respectively. The initial POD value is taken to be 10^{-4}.

3 Results and Discussion

3.1 OMI /MLS comparison for with and without PMCs

The ozone profile comparisons between OMI without retrieving PMCs and MLS are performed for two polar summer seasons, the North Hemisphere (NH), July 2007 and the South Hemisphere (SH), January 2008 when the PMC occurrence is most frequent in a given year. The comparison is limited to the high-latitude regions 75˚N-85˚N and 75˚S-85˚S. The vertical range is limited to pressures larger than 0.1 hPa due to the weak vertical ozone information from OMI measurements above; the retrieval could be adequately resolved below ~0.5 hPa in the stratosphere based on the averaging kernels (not shown here). In addition, MLS data have much larger uncertainties for ozone retrievals above 0.1 hPa as mentioned in Sect. 2.1. The collocated OMI and MLS measurements are separated into PMC and non-PMC pixels using the OMI PMC detection flag specified in Sect. 2.2. In order to reduce the effect of the OMI smoothing errors on the comparison, the high-resolution MLS data are convolved with the OMI averaging kernels. The upper panels of figure 1 compare the OMI and MLS ozone profiles averaged over PMC and non-PMC regions, respectively, on MLS pressure grids. The mean original/smoothed MLS profiles show no difference due to the presence of PMCs, but the differences become significant for the mean OMI profiles in the upper stratosphere. This demonstrates that the MLS stratospheric ozone product could be a proper reference for the evaluation of impacts of PMCs on OMI ozone retrievals during a PMC season. Despite the large relative biases (~ -20 % at 0.5 hPa) due to the presence of PMCs, the absolute bias is very small (~-0.05 DU at 0.5 hPa) because the ozone values in upper layers are quite small (Figure 1 c and d). It implies that the effect of PMCs on total ozone retrievals is negligible.

Figure 2 shows the mean biases and standard deviations of relative differences between OMI and smoothed MLS ozone profiles. With non-PMC pixels the maximum negative bias of OMI relative to MLS reaches -13% for the NH and -6% for the SH, respectively, at ~0.5 hPa. This bias increases to -30% for the NH and -24% for the SH when there are PMCs. The mean bias difference between PMC and non-PMC is the difference between the black and green lines in Fig. 1, almost the same as the black line since the MLS PMC/non-PMC difference is almost zero. We can see that the PMC effect on OMI retrievals starts at ~6 hPa (~35 km), leading to erroneous ozone reductions of ~20% at 0.5 hPa and ~2% at 2 hPa, similarly for both hemispheres. If we account for the occurrence frequency of PMCs, the overall PMC effect on average ozone at 0.5 hPa is

7.1 % ($20\,\% \times 2268/6388$) in the NH as there are ~ 2268 PMC pixels among 6388 pixels. This overall effect is three times larger compared to 2.3 % ($20\,\% \times 792/6808$) in the SH.

These PMC-induced ozone errors for OMI are more significant compared to ~10% error in individual SBUV ozone retrievals based on the SBUV version 5 algorithm (Thomas et al., 1991) and mean errors of up to 2-3 % in SBUV/2 ozone retrievals based on the SBUV version 8.6 algorithm (Bhartia et al., 2013). That is because the OMI ozone algorithm uses more wavelengths (270-330 nm) than SBUV algorithms (12 discrete wavelength bands between 240 and 340 nm), which are sensitive at PMCs. The spatial resolution of OMI, 48 km × 13 km is much smaller than SBUV (200 km × 200 km) and SBUV/2 (170 km × 170 km), so OMI has more chance to see a brighter PMC, resulting in a larger impact on ozone retrievals. In addition, the comparison of standard deviations shows almost no difference, indicating that the presence of PMCs mainly causes systematic retrieval biases.

In Fig. 3, OMI/MLS biases are plotted as functions of the PMC albedo residuals at 267 nm for the NH polar summer. This figure emphasizes that brighter PMCs have greater impact on the upper atmospheric ozone retrievals from UV measurements. The OMI-MLS differences increase up to 60-80% at the topmost three layers when PMCs are very bright. For dark PMC pixels, OMI retrievals agree well with MLS (mean biases are close to zero), except for negative biases of -20% in 0.15-0.46 hPa and -10% in 0.68-1.0 hPa. Observations from the Cloud Imaging and Particle Size (CIPS) instrument on the Aeronomy of Ice in the Mesosphere (AIM) satellite show that faint PMCs below the OMI detection threshold, with brightness as low as 1.0×10^{-6} sr^{-1}, are observed in 80-90% of all samples at 80° latitude (Lumpe et al., 2013). Thus, even pixels that are “dark” based on the OMI detection threshold may still have enough PMC contamination to bias OMI ozone retrievals above 1.0 hPa. A strong negative correlation of more than 0.5 is found in partial ozone columns above 2 hPa and no correlation (<0.1) at those layers below 6 hPa. This similar behavior is detected for the relationship between biases due to PMCs and albedo residuals in the SH polar summer presented in Table 1.

3.2 Sensitivity of UV radiances to PMCs

In Fig. 4.a, the sensitivity of OMI radiance to POD ranging from 10^{-5} to 10^{-3} is plotted as functions of wavelength for a SZA of 70°, VZA of 45° and AZA of 135°. Despite being optically thin, PMCs can significantly affect the UV radiances at shorter wavelengths where the signal is weak, implying that the effect of PMC scattering may be not negligible for the stratospheric ozone retrievals from OMI as well as the SBUV, SBUV/2, GOME, GOME-2, SCIAMACHY, and OMPS Nadir Profiler instruments. The presence of PMCs with the optical depth of 10^{-3} enhances the radiances from 2% at 300 nm to 8% at 265 nm for AZA of 135°. This sensitivity increases 4 times for the same SZA and VZA but AZA of 45° (Fig. 4.b). Furthermore, it is shown that POD should be larger than ~10^{-4} for the case in Fig. 4.a and larger than ~2×10^{-5} in Fig. 4.b to be detectable from UV measurements as the OMI measurement errors at ~270 nm are ~1%.

Figure 4.c shows the viewing geometry dependence of PMC sensitivity at 267 nm. The sensitivity varies largely with SZA, VZA, and AZA, except that at AZA larger than 90° the dependence on viewing geometry becomes relatively insignificant. This dependence on AZA is mainly due to the steeper phase function variation of PMCs at forward scattering angles, displayed in Fig. 4.d. The significant increase in PMC sensitivity with larger SZA or VZA at AZA < 90° is mainly due to the larger photon path length for PMC scattering. Overall, the dependence on viewing geometry is a direct result of the strength of the PMC scattering.

Sensitivity studies using the optimal estimation formulation (with a loose PMC a priori constraint of 10^{-3}) show that POD can be retrieved with errors from $1 - 6.5 \times 10^{-4}$ depending on viewing geometry, as shown in Fig. 5. The POD retrieval errors are smaller at longer slant paths and smaller AZAs where the scattering is stronger and sensitivity becomes larger. As we mentioned in Sect. 2.2 the typical AZA for OMI PMC detection varies from 40° to 130° (SZAs >35°, latitude >55°N/S) and thereby the errors of OMI POD retrievals are expected to have significant dependence on the scattering angle.

Figure 6 shows the impact of PMCs on ozone profile retrievals due to the neglect of PMCs, estimated as $\frac{\partial \widehat{x_{O3}}}{\partial Y} \cdot \frac{\partial Y}{x_{POD}} \cdot \Delta POD$. This result is generally consistent with the effect of PMCs on the OMI and MLS comparisons shown in Figs 1-2: The presence of PMCs results in negative ozone retrieval errors above 6 hPa, the ozone errors increase rapidly up to ~0.5 hPa and continue to increase with the greatest peak impact at 0.2 hPa (60 km). At AZA = 135° (Fig. 6.a) ozone errors increase -2.5% for POD of 10^{-4} to -25% for POD of 10^{-3}. These ozone retrieval errors are expected to increase at longer slant paths and smaller AZAs. For example, as shown in Fig. 6.b, the errors increase by a factor of 5 when the AZA is changed to 45°.

3.3 Simultaneous retrievals of ozone profile and PMC optical depth

As mentioned in Sect. 2.3, the POD a priori value and its error are determined as 0 and 10^{-3}, respectively, by trial and error. The POD initial value of 10^{-4} is close to the minimum value that is detectable from UV radiances below 300 nm as shown in Figs. 4. a and b. An example for POD retrieved from OMI nadir measurements with three a priori errors is presented in Fig. 7. This example illustrates that the a priori error value of 10^{-4} is a very tight constraint as the retrieved POD values are very small for both PMC and non-PMC pixels. This also indicates that the POD can be consistently retrieved from measurement information with a priori error values $\geq 10^{-3}$, implying that the degree of freedom for signal is close to 1 for the POD parameter. The retrieved optical depths are generally larger at PMC pixels than at non-PMC pixels. Furthermore, the significant correlation (r=~ 0.8) between POD and albedo residuals is demonstrated in Fig. 8. The typical value of the retrieved optical depth is around $1-5\times 10^{-4}$ and increases up to 15×10^{-4} for bright PMC pixels. Solution errors for PMC increase from 1×10^{-4} at larger SZAs to 4×10^{-4} at smaller SZAs. These retrieval errors are distinctly smaller than the a priori error of 10^{-3}. This result are consistent with the sensitivity studies as shown in Fig. 5, considering the AZAs for OMI measurements used in Fig. 7 vary from 61° and 89° and VZAs are within 11°.

Figure 8b compares the retrieved ozone columns above 40 km with and without including the POD in the state vector. It illustrates that the retrieved ozone values tend to be larger if the PODs are simultaneously retrieved because of slight anticorrelation between POD and ozone parameters in the upper atmosphere. The ozone column differences are larger for PMC pixels than for non-PMC pixels, indicating that the simultaneously retrieved POD could correct the negative biases in OMI ozone retrievals. However, there are non-PMC pixels that show significant correlation between the POD and ozone parameters at SZAs 57°-67°, indicating that some PMC pixels are not detected from OMI. Figure 9 and 10 evaluate the improvements of OMI/MLS ozone profile comparisons with the simultaneous retrievals of POD and ozone. The systematic biases due to PMCs are mostly corrected, especially for bright PMC pixels: the negative biases range from 15% to 50% depending on the PMC albedo residuals in the upper atmosphere, but are reduced to within ±10% below 1-2 hPa. The significant negative correlation between OMI/MLS ozone differences and PMC albedo residuals found in Figure 3 is reduced to within 0.1 in most layers, except for the topmost two layers (R=-0.25). However, the simultaneous ozone/POD retrievals systematically show positive biases (~ 10%) for the layers of 1.21-2.15 hPa relative to MLS data, irrespective of albedo residuals, and even for non-PMC pixels.

4. Summary and Discussion

This work demonstrats the interference of tenuous PMCs on OMI ozone profile retrievals above 6 hPa. The presence of PMCs leads to the systematic biases of -2% at 2 hPa and -20% at 0.5 hPa for pixels with PMCs in both hemispheres; however, the overall impact on the average ozone in the NH are three times larger than that in the SH if the PMC occurrence frequency is considered. The magnitude of systematic biases can increase to up to ~60 - 80% for very bright PMC pixels. Despite the large relative biases in the upper atmosphere, the impact of PMCs on our retrieved total ozone (~305 DU for the NH summer polar region) is negligible with the absolute biases of ~ 0.05 DU at 0.5 hPa.

Sensitivity analysis shows that the PMC sensitivity is strongly dependent on wavelength, larger at shorter wavelengths where the signals are weak. PMC sensitivity is also strongly dependent on viewing geometry in the forward scattering direction (e.g., relative azimuth angles less than 90°); PMC sensitivity increases with larger SZAs and VZAs due to longer path lengths for PMC scattering and especially with smaller AZAs due to much stronger forward scattering. For AZAs greater than 90°, the dependence becomes insignificant because the PMC scattering varies much less with viewing geometry. PMC optical depth of $\sim 10^{-4}$ is detectable from OMI data in the back scattering direction and the PMC detection limit could be smaller for the forward scattering direction. The maximum contribution of ignoring PMC to ozone retrievals is found at ~0.2 hPa.

To reduce PMC interference on upper level ozone retrievals, we added the PMC optical depth (POD) to the state vector in the OMI optimal estimation ozone profile algorithm. The PMC a priori value and a priori error are set at 0 and 10^{-3}, respectively in this study. The selected a priori error value corresponds to a loose constraint, implying that the retrieved optical depth comes mainly from measurement information. As a result, the POD can be retrieved with uncertainties of $1-4\ \times 10^{-4}$ depending on solar zenith angle. A near-linear relationship is found between POD and albedo residuals (R~0.8); the retrieved POD values are $1-5\ \times 10^{-4}$ at dark PMC pixels and increase up to $15\ \times 10^{-4}$ for bright PMC pixels. It is demonstrated that the simultaneous retrieval of POD could improve the OMI and MLS comparisons. The negative OMI biases are reduced to within ±10% after simultaneous ozone/POD retrievals. In addition, this simultaneous retrieval reduces the strong negative correlation between OMI/MLS biases and PMC albedo residuals to ~0.1 above 2 hPa, which is found to be stronger than -0.5 for ozone retrieval only. However, there are some non-PMC pixels where large POD values are retrieved and hence are correlated with ozone parameters, which might represent undetected PMC pixels from OMI UV measurements.

This study indicates that the impact of PMC scattering is likely not negligible for stratospheric ozone retrievals from OMI, SBUV, SBUV/2, GOME, GOME-2, SCIAMACHY, and OMPS Nadir Profiler as the effects of PMCs have not been taken into account in any of the operational ozone profile algorithms. The presence of PMCs has greater influence on our OMI ozone retrievals compared to the PMC-induced errors on SBUV and SBUV/2 ozone retrievals shown in Thomas et al., (1991) and Bhartia et al. (2013), which could be explained by OMI having more chances to see brighter PMC pixels due to its much smaller pixel size and by our algorithm using continuous wavelengths of 270-330 nm whereas the SBUV algorithms use several discrete wavelength bands between 240 and 340 nm. In addition, the different ozone retrieval algorithms have different sensitivity to PMC contamination. For example, PMC-induced errors in Nimbus-7 SBUV ozone data based on the NASA Version 5 algorithm (McPeters et al, 1980) can be as large as 10 %. Recently, Bhartia et al. (2013) did some analysis of PMC effects on NOAA-18 SBUV/2 ozone data using the NASA Version 8.6 algorithm and found that the average effects are typically in the 2-3% range. Likewise, the OMI operational ozone profile product, OMO3PR (Kroon et al., 2011) has different response to PMC contamination due to different implementation details although it is also based on optimal estimation with the same fitting window; the comparison between two OMI algorithms has been described in Bak et al., (2015). We compare the OMO3PR ozone product between PMC and non-PMC pixels, similarly to Fig. 1.a (not shown here). The impact of PMCs on the OMO3PR product is comparable to our ozone retrievals below 0.1 hPa, but becomes smaller above them with erroneous ozone reduction of ~ 10% at 0.5 hPa. This smaller impact is likely due to fitting of second-order polynomial radiance offsets to account for stray lights [Personal communication, P. Veefkind], which is not used in our algorithm. The impact of PMCs on total ozone retrievals such as OMTO3 (Bhartia and Wellemeyer, 2002) and OMDOAO3 (Veefkind et al., 2006) are negligible because the total ozone algorithms use longer wavelengths than 310 nm where the PMC signal is very weak and the impacts of PMCs on the ozone columns are too small to affect the total ozone retrievals.

Acknowledgements The authors thank the OMI and MLS science teams for providing the satellite data. Research at Pusan National University by J. Bak and J.H. Kim was supported by the Eco Innovation Program of KEITI (2012000160002), South Korea. Research at the Smithsonian Astrophysical Observatory by X. Liu, and K. Chance, as well as J. Bak during her 3-month visit to Harvard-Smithsonian was funded by NASA Aura science team program (NNX11AE95G and NNX14AF16G) and the Smithsonian Institution.

References

Bailey, S. M., Merkel, A. W., Thomas, G. E., and Carstens, J. N.: Observations of polar mesospheric clouds by the Student Nitric Oxide Explorer, J. Geophys. Res., 110, D13203, doi:10.1029/2004JD005422, 2005.

Bak, J., Liu, X., Kim, J. H., Chance, K., and Haffner, D. P.: Validation of OMI total ozone retrievals from the SAO ozone profile algorithm and three operational algorithms with Brewer measurements, Atmos. Chem. Phys., 15, 667-683, doi:10.5194/acp-15-667-2015, 2015.

Baumgarten, G. and Thomas, G. E.: The importance of ice particle shape on UV measurements of polar mesospheric clouds: SBUV/2 observations, J. Atmos. Sol. Terr. Phys., 68(1), 78 – 84, doi:10.1016/j.jastp.2005.08.007, 2006.

Bhartia, P. K. and Wellemeyer, C.: TOMS-V8 total O3 algorithm, in OMI Algorithm Theoretical Basis Document, vol. II, OMI Ozone Products, ATBD-OMI-02, edited by P. K. Bhartia, pp. 15matology (vs. 20% Space Flight Cent., Greenbelt, Md., available at http://eospso.gsfc.nasa.gov/eos_homepage/for_scientists/atbd/index.php, 2002.

Bhartia, P. K., McPeters, R. D., Flynn, L. E., Taylor, S., Kramarova, N. A., Frith, S., Fisher, B., and DeLand, M.: Solar Backscatter UV (SBUV) total ozone and profile algorithm, Atmos. Meas. Tech., 6, 2533-2548, doi:10.5194/amt-6-2533-2013, 2013.

DeLand, M. T., Shettle, E. P., Thomas, G. E., and Olivero, J. J.: Solar backscattered ultraviolet (SBUV) observations of polar mesospheric clouds (PMCs) over two solar cycles, J. Geophys. Res., 108, 8445, doi: 10.1029/2002JD002398, 2003.

DeLand, M. T., Shettle, E. P, Thomas, G. E., and Olivero, J. J.: A quarter-century of satellite PMC observations, J. Atmos. Sol. Terr. Phys., 68, 9–29, doi:10.1016/j.jastp.2005.08.003, 2006.

DeLand, M. T., Shettle, E. P, Thomas, G. E., and Olivero, J. J.: Latitude-dependent long-term variations in polar mesospheric clouds from SBUV version 3 PMC data, J. Geophys. Res., 112, D10315, doi:10.1029/2006JD007857, 2007.

DeLand, M. T., Shettle, E. P., Levelt, P. F., and Kowalewski M. G.: Polar Mesospheric Clouds (PMCs) Observed by the Ozone Monitoring Instrument (OMI) on Aura, J. Geophys. Res., 115, D21301, doi:10.1029/2009JD013685, 2010.

DeLand, M. T., Shettle, E. P, Thomas, G. E., and Olivero, J. J.: Direct observations of PMC local time variations by Aura OMI, J. Atmos. Sol. Terr. Phys., 73, 2049–2064, doi:10.1016/j.jastp.2010.11.019, 2011.

DeLand, M. T., and Thomas, G. E.: Updated PMC trends derived from SBUV data, J. Geophys. Res. Atmos., 120, doi:10.1002/2014JD022253, 2015.

Englert, C. R., and Stevens, M. H.: Polar mesospheric cloud mass and the ice budget: 1. Quantitative interpretation of mid-UV cloud brightness observations, J. Geophys. Res., 112, 08204, doi: 10.1029/2006JD007533, 2007.

Eremenko, M. N., Petelina, S. V., Zasetsky, A. Y., Karlsson, B. , Rinsland, C. P., Llewellyn, E. J., and Sloan, J. J.: Shape and composition of PMC particles derived from satellite remote sensing measurements, Geophys. Res. Lett., 32, L16S06, doi:10.1029/2005GL023013, 2005.

European Space Agency (ESA): The GOME Users Manual, ESA Publ. SP-1182, Publ. Div., Eur. Space Res. and Technol. Cent., Noordwijk, Netherlands, 1995.

Flynn, L., long, C., Wu, X., Evans, R., Beck, C. T., Petropavlovskikh, I., McConville, G., Yu, W., Zhang, Z., Niu, J., Beach, E., Hao, Y., Pan, C., Sen, B., Novicki, M., Zhou, S., and Seftor, C. : Performance of the Ozone Mapping and Profiler Suite (OMPS) products, J. Geophys. Res. Atmos., 119, 6181–6195, doi:10.1002/2013JD020467, 2014.

Hervig, M., Thompson, R. E., McHugh, M., Gordley, L. L., Russell III, J. M., and Summers , M. E.: First confirmation that water ice is the primary component of polar mesospheric clouds, Geophys. Res. Lett., 28, 971–974, 2001.

Hervig, M. E., Gordley, L. L., Stevens, M. H., Russell III, J. M., Bailey, S. M., and Baumgarten, G.: Interpretation of SOFIE PMC measurements: Cloud identification and derivation of mass density, particle shape, and particle size, J. Atmos. Solar Terr. Phys., 71, 316-330, 2009.

Hervig, M. E. and Stevens, M. H.: Interpreting the 35 year SBUV PMC record with SOFIE observations, J. Geophys. Res. Atmos., 119, 12,689–12,705, doi:10.1002/2014JD021923, 2014.

Kroon, M., de Haan, J. F., Veefkind, J. P., Froidevaux, L., Wang, R., Kivi, R., and Hakkarainen, J. J.: Validation of operational ozone profiles from the Ozone Monitoring Instrument, J. Geophys. Res., 116, D18305, doi: 10.1029/2010JD015100, 2011.

Levelt, P. F., van den Oord, G. H. J., Dobber, M. R., Malkki, A., Visser, H., de Vries, J., Stammes, P., Lundell, J. O. V., and Saari, H.: The Ozone Monitoring Instrument, IEEE Trans. Geosci. Remote Sens., 44(5), 1093–1101, doi:10.1109/TGRS.2006.872333, 2006.

Liu, X., Bhartia, P.K, Chance, K, Spurr, R.J.D., and Kurosu, T.P.: Ozone profile retrievals from the ozone monitoring instrument, Atmos. Chem. Phys., 10, 2521-2537, doi:10.5194/acp-10-2521-2010, 2010a.

Liu, X., Bhartia, P. K., Chance, K., Froidevaux, L., Spurr, R. J. D., and Kurosu, T. P.: Validation of Ozone Monitoring Instrument (OMI) ozone profiles and stratospheric ozone columns with Microwave Limb Sounder (MLS) measurements, Atmos. Chem. Phys., 10, 2539-2549, doi:10.5194/acp-10-2539-2010, 2010b.

Livesey, N. J., Read, W. G., Froidevaux, L., Lambert, A., Manney, G. L., Pumphrey, H. C., Santee, M. L., Schwartz, M. J., Wang, S., Cofeld, R. E., Cuddy, D. T., Fuller, R. A., Jamot, R. F., Jiang, J. H., Knosp, B. W., Stek, P. C., Wagner, P. A., and Wu, D. L.: Version 3.3 Level 2 data quality and description document, JPL California Institute of Technology, Pasadena, California, 91109–8099, 2011.

Lumpe, J. D., Bailey, S. M., Carstens, J. N., Randall, C. E., Rusch, D. W., Thomas, G. E., Nielsen, K., Jeppesen, C., McClintock, W. E., Merkel, A. W., Riesberg, L., Templeman, B., Baumgarten, G., and Russell III, J. M.: Retrieval of polar mesospheric cloud properties from CIPS: Algorithm description, error analysis and cloud detection sensitivity, J. Atmos. Solar-Terr. Phys., 104, 167-196, 2013.

McPeters, R. D.: The Behavior of Ozone near the Stratopause from 2 Years of BUV Observations, J. Geophys. Res.-Oc. Atm., 85, 4545–4550, 1980.

McPeters, R. D. and Labow, G. J.: Climatology 2011: an MLS and sonde derived ozone climatology for satellite retrieval algorithms, J. Geophys. Res., 1117, 10303, doi:10.1029/2011JD017006, 2012.

Munro, R., Eisinger, M., Anderson, C., Callies, J. , Corpaccioli, E. , Lang, R., Lefebvre, A., Livschitz, Y., and Pérez Albiñana, A. : GOME-2 on MetOp, paper presented at the 2006 EUMETSAT Meteorological Satellite Conference, Eur. Org. for the Exploit. of Meteorol. Satell., Helsinki, 2006.

Rapp, M., Thomas, G. E., and Baumgarten, G.: Spectral properties of mesospheric ice clouds: Evidence for nonspherical particles, J. Geophys. Res., 112, D03211, doi:10.1029/2006JD007322, 2007.

Rodgers, C. D.: Inverse Methods for Atmospheric Sounding: Theory and Practice, World

Scientific Publishing, Singapore, 2000.
Olivero, J. J., and Thomas, G. E.: Climatology of polar mesospheric clouds, J. Atmos. Sci., 43, 1263– 1274, 1986.
Shettle, E. P, DeLand, M. T., Thomas, G. E., and Olivero, J. J.: Long term variations in the frequency of polar mesospheric clouds in the Northern Hemisphere from SBUV, Geophys. Res. Lett., 36, 02803, doi: 10.1029/2008GL036048. 2009.
Schoeberl, M.R.; Douglass, A.R.; Hilsenrath, E.; Bhartia, P.K.; Beer, R.; Waters, J.W.; Gunson, M.R.; Froidevaux, L.; Gille, J.C.; Barnett, J.J.; Levelt, P.F.; DeCola, P.: Overview of the EOS aura mission, IEEE Transactions on Geoscience and Remote Sensing, 44(5), 1066-1074, doi: 10.1109/TGRS.2005.861950, 2006.
Spurr, R. J. D.: VLIDORT: A linearized pseudo-spherical vector discrete ordinate radiative transfer code for forward model and retrieval studies in multilayer multiple scattering media, J. Quant. Spectrosc. Ra., 102, 316–342, 2006.
Spurr, R. J. D.: Linearized pseudo-spherical scalar and vector discrete ordinate radiative transfer models for use in remote sensing retrieval problems, in: Light Scattering Reviews, edited by: Kokhanovsky, A., Springer, New York, 2008.
Taylor, M. J., Gadsden, M., Lowe, R. P., Zalcik, M. S., and Brausch, J.: Mesospheric cloud observations at unusually low latitudes, J. Atmos. Solar Terr. Phys., 64, 991-999, 2002.
Thomas, G.E.: Solar mesosphere explorer measurements of polar mesospheric clouds (noctilucent clouds). Journal of Atmospheric and Terrestrial Physics, 46, 819–824, doi:10.1016/0021-9169(84)90062-X, 1984.
Thomas, G. E., McPeters, R. D. and Jensen, E. J.: Satellite observations of polar mesospheric clouds by the solar backscattered ultraviolet spectral radiometer - Evidence of a solar cycle dependence, J. Geophys. Res., 96, 927-939, 1991.
von Savigny, C., Kokhanovsky, A., Bovensmann, H., Eichmann, K.-U., Kaiser, J., Noel, S., Rozanov, A. V., Skupin, J., and Burrows, J. P.: NLC detection and particle size determination: first results from SCIAMACHY on Envisat, Adv. Space Res., 34, 851-856, 2004.

von Savigny, C., and Burrows, J. P.: Latitude variation of NLC particle radii derived from northern hemisphere SCIAMACHY/Envisat limb measurements, Adv. Space Res., 40, 765-771, 2007.

Veefkind, J. P., De Haan, J. F., Brinksma, E. J., Kroon, M., and Levelt, P. F.: Total ozone from the ozone monitoring instrument (OMI) using the DOAS technique, IEEE Trans. Geosci. Remote Sens., 44(5), 1239-1244, doi: 10.1109/TGRS.2006.871204, 2006.

Warren, S., G.: Optical constants of ice from the ultraviolet to the microwave, Applied Optics, Vol. 23, Issue 8, pp. 1206-1225, http://dx.doi.org/10.1364/AO.23.001206, 1984

Waters, J.W.; Froidevaux, L.; Harwood, R.S.; Jarnot, R.F.; Pickett, H.M.; Read, W.G.; Siegel, P.H.; Cofield, R.E.; Filipiak, M.J.; Flower, D.A.; Holden, J.R.; Lau, G.K.; Livesey, N.J.; Manney, G.L.; Pumphrey, H.C.; Santee, M.L.; Wu, D.L.; Cuddy, D.T.; Lay, R.R.; Loo, M.S.; Perun, V.S.; Schwartz, M.J.; Stek, P.C.; Thurstans, R.P.; Boyles, M.A.; Chandra, K.M.; Chavez, M.C.; Gun-Shing Chen; Chudasama, B.V.; Dodge, R.; Fuller, R.A.; Girard, M.A.; Jiang, J.H.; Yibo Jiang; Knosp, B.W.; LaBelle, R.C.; Lam, J.C.; Lee, K.A.; Miller, D.; Oswald, J.E.; Patel, N.C.; Pukala, D.M.; Quintero, O.; Scaff, D.M.; Van Snyder, W.; Tope, M.C.; Wagner, P.A.; Walch, M.J., "The Earth observing system microwave limb sounder (EOS MLS) on the aura Satellite," in Geoscience and Remote Sensing, IEEE Transactions on , vol.44, no.5, pp.1075-1092, May 2006, doi: 10.1109/TGRS.2006.873771, 2006.

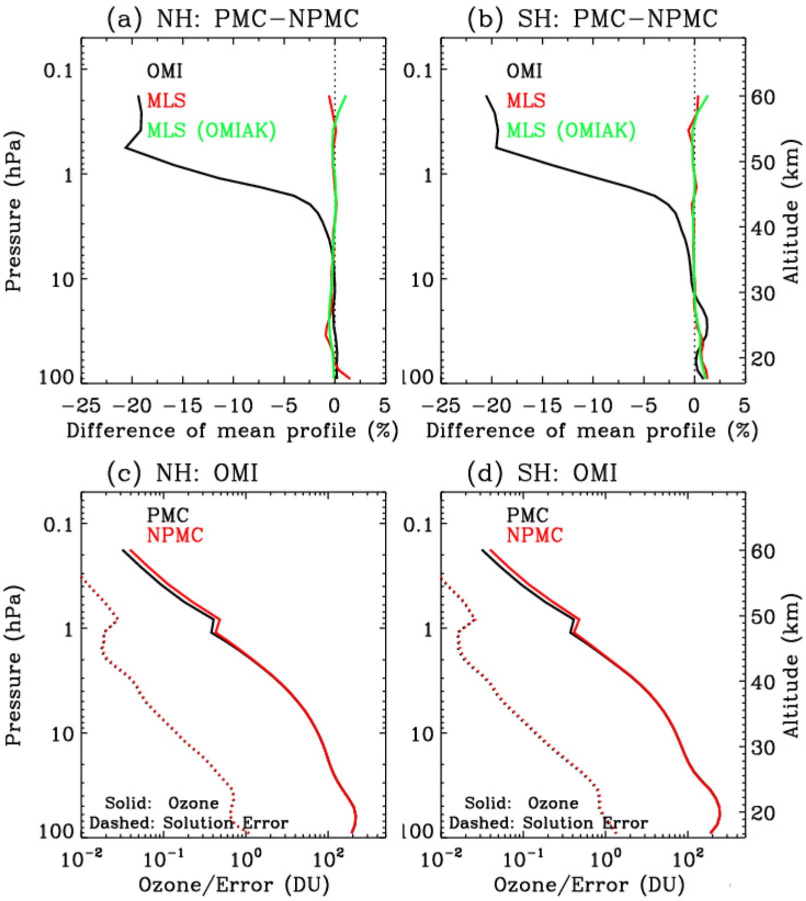

Figure 1. Difference of mean ozone profiles from OMI (black), collocated MLS (red), and MLS convolved with OMI averaging kernels (green) between PMC and non-PMC pixels (($\mathbf{PMC - NPMC}$)/NPMC $\times \mathbf{100}$ %) (upper panels), with OMI ozone (solid lines) and solution error (dashed line) profiles averaged over PMC and non-PMC pixels, respectively (lower panels). (a, c) and (b, d) are results from NH 2007 (July 2007, 75˚N-85˚N) and SH 2008 (January 2008, 75˚S-85˚S) summer seasons, respectively.

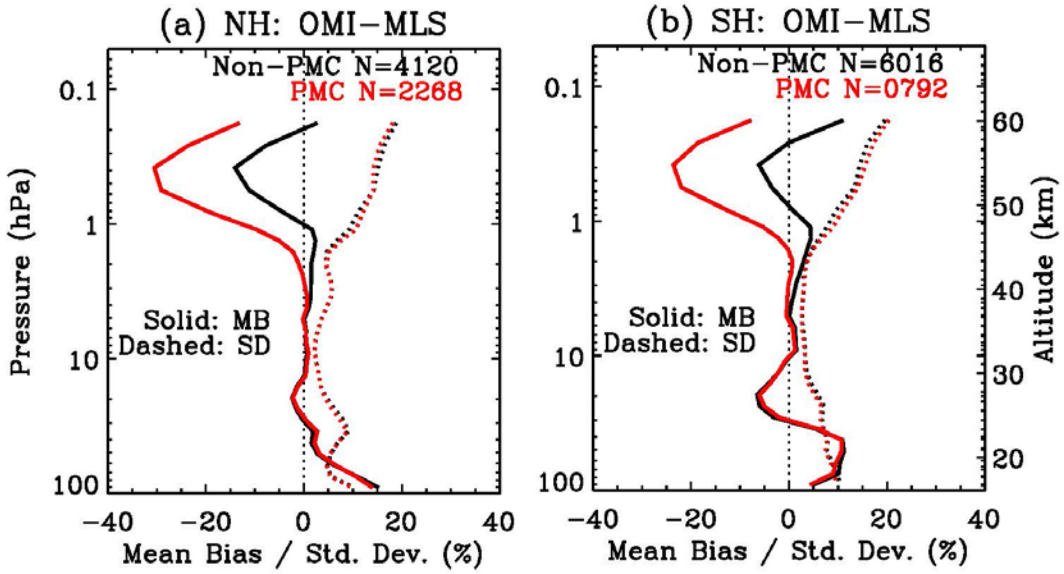

Figure 2. Same as Figure 1, but for the mean differences (solid lines) between OMI and collocated MLS convolved with OMI averaging kernels, (OMI-MLS)/OMI a priori$\times$ $\mathbf{100}$%, and their 1σ standard deviations (dashed lines) for PMC (red) and non-PMC (black) pixels. The number of collocations (N) is shown in the legend.

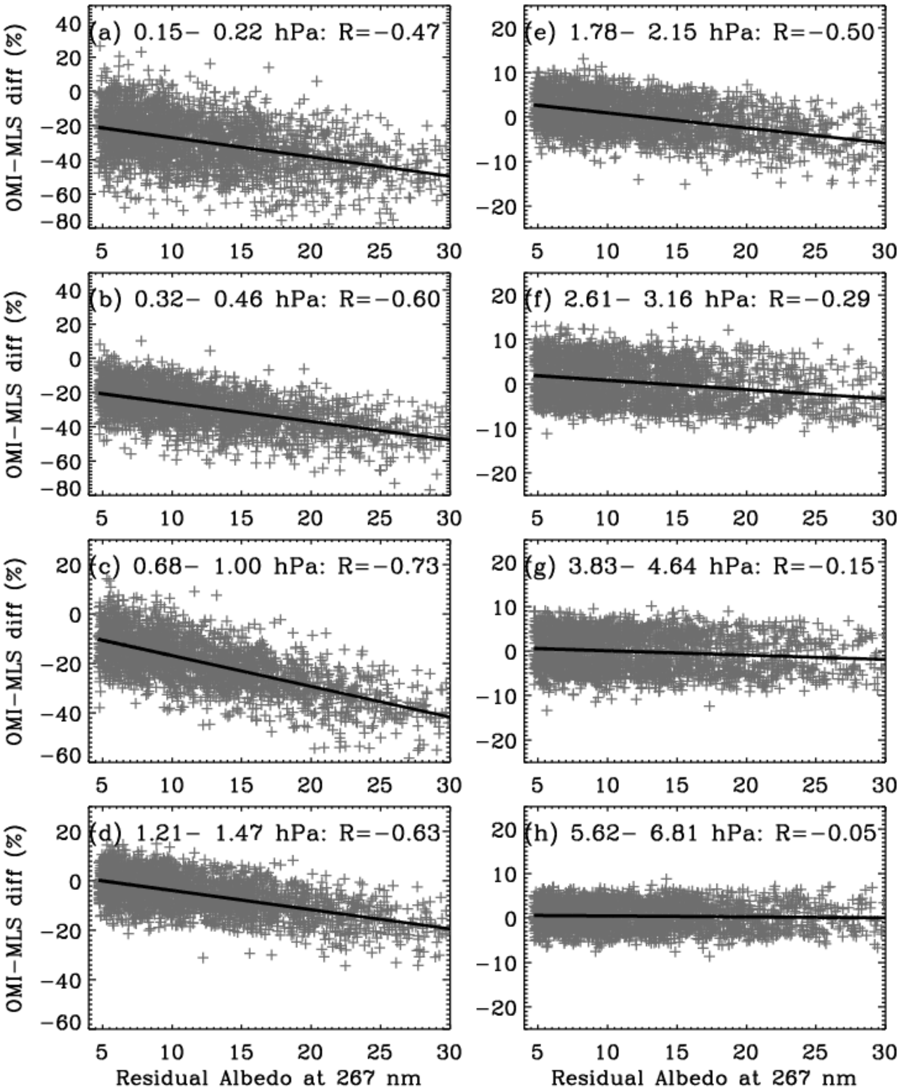

Figure 3. Scatter plots between OMI/convolved MLS partial column ozone difference (%) for eight MLS layers and PMC albedo residual at 267 nm (**× 10^{-6} sr^{-1}**) for NH 2007 summer. The correlation coefficients (R) are shown in the legend.

Table 1. Correlation between OMI/convolved MLS ozone differences and PMC albedo residuals at 267nm as shown in Figure 3, but for SH 2008 summer.

Layer (hPa)	Correlation	Layer (hPa)	Correlation
0.15-0.22	-0.42	1.78-2.15	-0.49
0.32-0.46	-0.57	2.61-3.16	-0.36
0.68-1.00	-0.59	3.83-4.64	-0.27
1.21-1.47	-0.54	5.62-6.81	-0.14

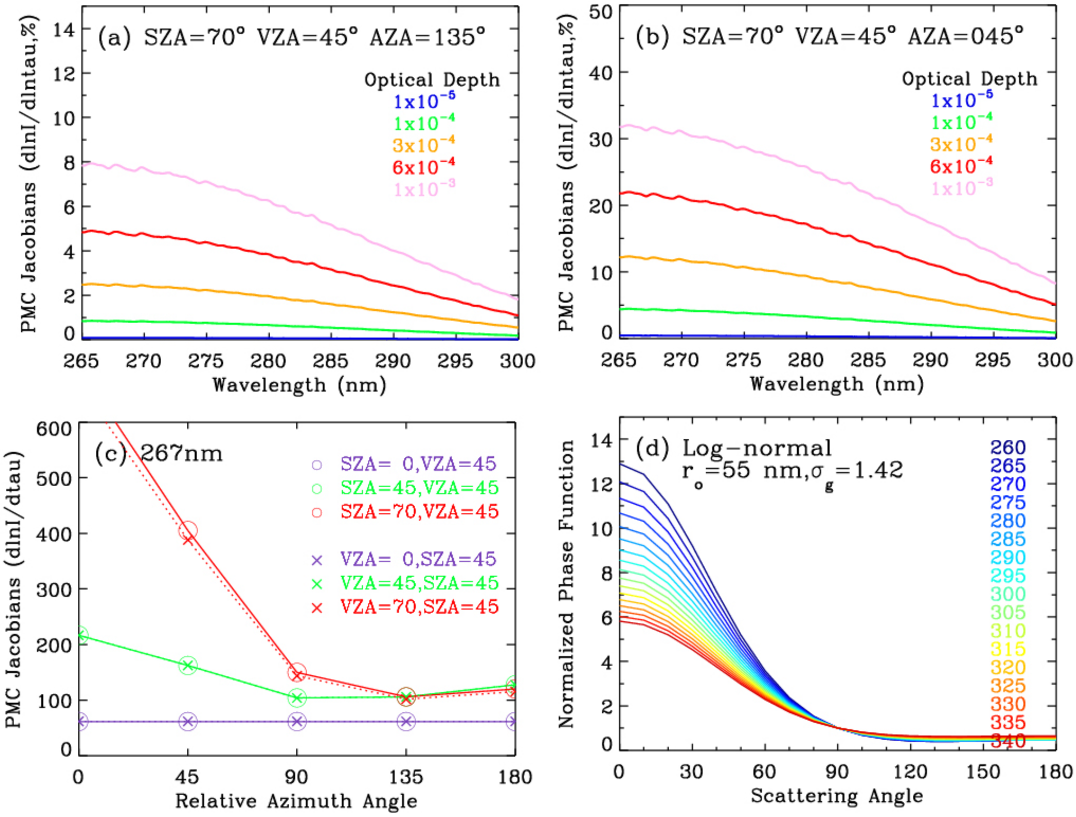

Figure 4. (a) Jacobians with respect to PMC optical depth ("tau") as functions of wavelength at SZA =70°, VZA= 45°, and AZA=135° for five optical depth values ranging from 10^{-5} to 10^{-3}. (b) Same as (a), but for AZA=45°. (c) Normalized PMC Jacobians at 267 nm as a function of AZA with various SZAs and VZAs. (d) PMC phase function as a function of scattering angle (**Φ**) for wavelengths ranging from 260 to 340 nm, normalized to unity at $\mathbf{\Phi = 90}$°.

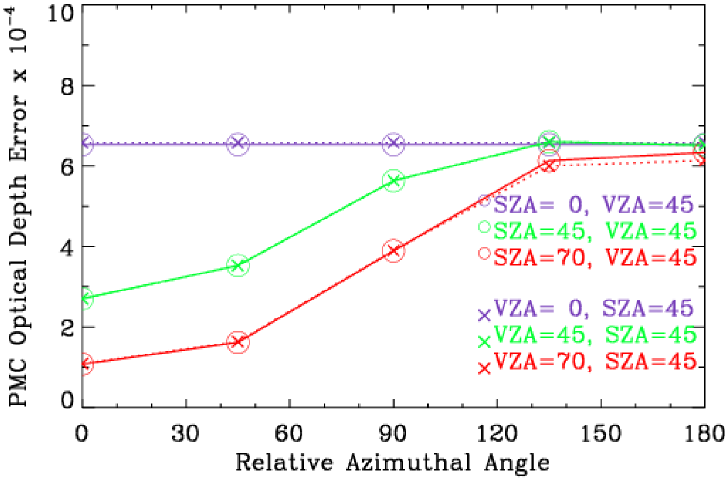

Figure 5. Same as Fig. 4.c, but for PMC optical depth retrieval errors (root sum square of random noise and smoothing errors).

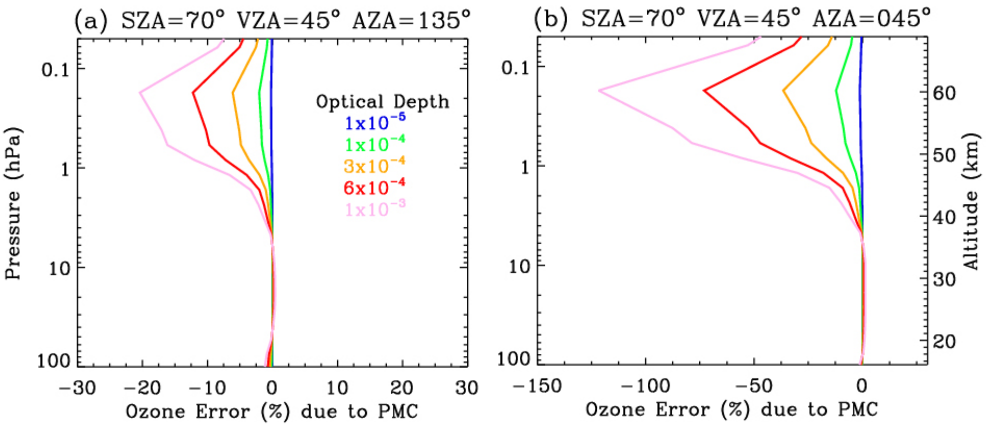

Figure 6. Ozone profile retrieval errors as functions of pressure due to the neglect of PMCs estimated based on the optimal estimation approach.

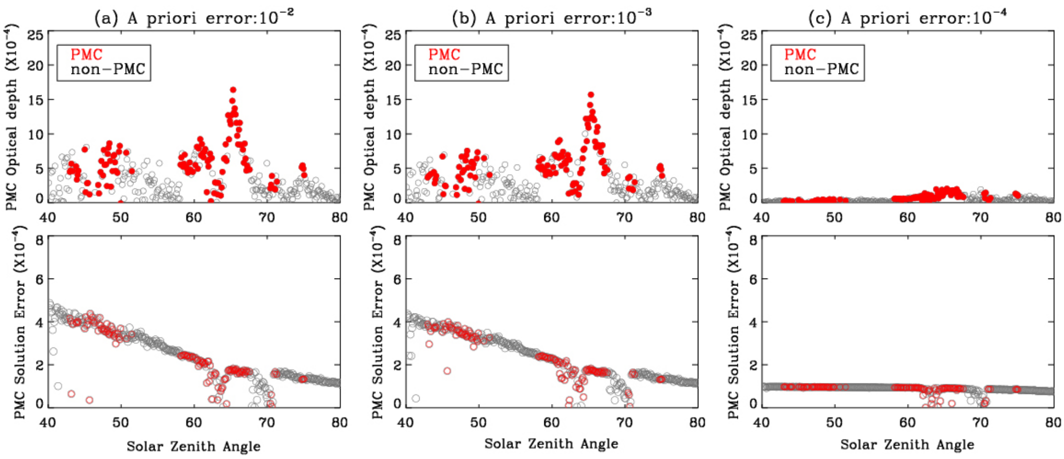

Figure 7. Retrieved PMC optical depth values and retrieval errors as functions of solar zenith angle for OMI orbit number 15881 and cross-track position 13 (UV1) with a fixed a priori value of 0 and three a priori error values, (a) 10^{-2}, (b) 10^{-3}, and (c) 10^{-4}, respectively.

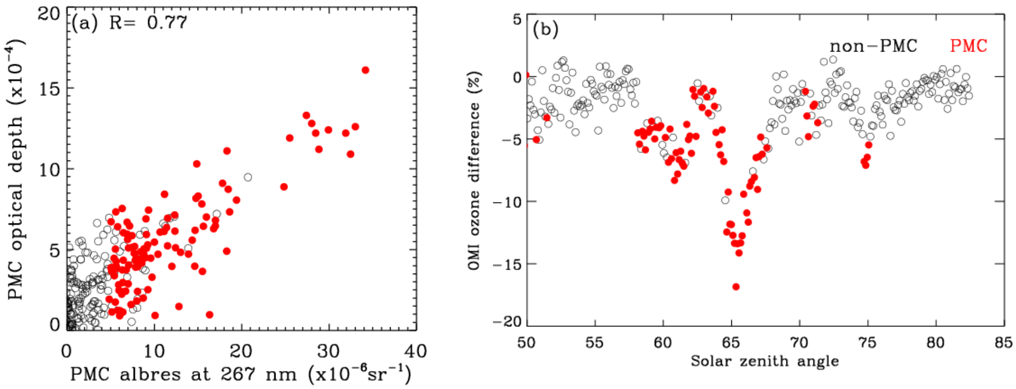

Figure **8**. (a) Scatter plot between retrieved PMC optical depths (POD) and PMC albedo residuals at 267 nm for OMI orbit number 15881 and cross-track position 13 (UV1). (b)

OMI ozone column (above 40 km) differences between “ozone only” and “ozone+POD” retrieval modes.

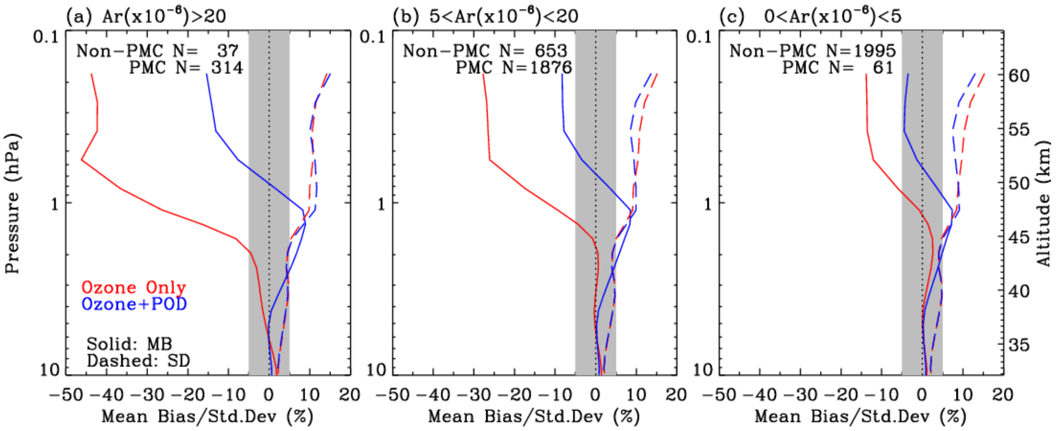

Figure 9. Collocated OMI/convolved MLS profile differences (solid lines) and their 1**σ** standard deviations (dashed lines) for different ranges of PMC albedo residual (Ar) values (sr^{-1}) at 267 nm for the NH 2007 summer season. The blue and red lines represent the comparisons when OMI ozone profiles are retrieved with and without PMC optical depths (PODs), respectively. The numbers of the Non-PMC and PMC pixels are included as legends.

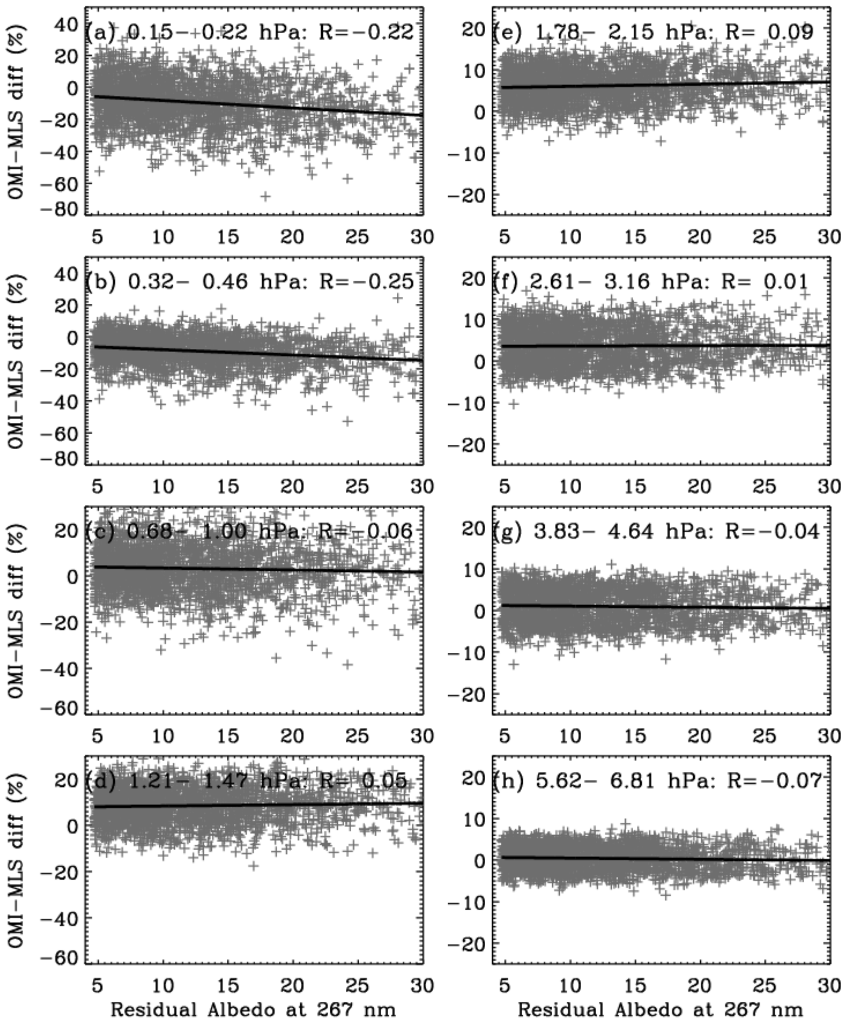

Figure 10. Same as Figure 3, but with PMC optical depths simultaneously retrieved with ozone.